Carbohydrate Polymers 83 (2011) 1740–1748

Contents lists available at ScienceDirect

Carbohydrate Polymers

journal homepage: www.elsevier.com/locate/carbpol

Water sorption behavior and gas barrier properties of cellulose whiskers and microfibrils films

Sabrina Belbekhouche[a], Julien Bras[b], Gilberto Siqueira[b], Corinne Chappey[a], Laurent Lebrun[a], Bertine Khelifi[b], Stéphane Marais[a], Alain Dufresne[b,*]

[a] PBS Rouen Université de Rouen, Laboratoire «Polymères, Biopolymères, Surfaces», UMR6270, FR3038, INC3M, 76821 Mont-Saint-Aignan Cedex, France
[b] Grenoble Institute of Technology (INP) – The International School of Paper, Print Media and Biomaterials (Pagora), BP 65, F-38402 Saint Martin d'Hères Cedex, France

ARTICLE INFO

Article history:
Received 8 July 2010
Received in revised form 12 October 2010
Accepted 19 October 2010
Available online 23 October 2010

Keywords:
Cellulose
Whiskers
Microfibrillated cellulose (MFC)
Sisal
Barrier properties

ABSTRACT

Rod-like straight cellulose whiskers and long flexible entangled microfibrillated cellulose (MFC), both extracted from sisal fibers, were used to prepare cellulosic membranes. In view of the promising barrier properties recently reported separately in the literature for these naturally occurring particles it was of interest to investigate the influence of the nature of the nanoparticles (whiskers *vs.* MFC) on the transport properties of the films. The water vapor and gas (carbon dioxide, nitrogen and oxygen) permeability of films composed of either cellulose nanocrystals or MFC has been reported. It was observed that the diffusion of water is rather controlled by the surface than by the core, probably because of a barrier effect related to the presence of water at the surface during the sorption kinetics. The cellulose whiskers film was found to be much more permeable to gases than MFC. This difference was ascribed to the higher porosity of the former and to the possibility of entanglements of MFC and different surface chemistry.

1. Introduction

The potential of nanocomposites in various sectors of research and application is promising and attracts increasing investments. Due to their abundance, high strength and stiffness, low weight and biodegradability, nano-scale cellulosic particles serve as promising candidates for the preparation of bionanocomposites. A broad range of applications of cellulosic nanoparticles exists even if a high number of unknown remains at date. Tens of scientific publications and experts show its potential even if most of the studies focus on their mechanical properties as reinforcing phase and their liquid crystal self-ordering properties (Azizi Samir, Alloin, & Dufresne, 2005; Dufresne, 2006; Hubbe, Rojas, Lucia, & Sain, 2008; Siró & Plackett, 2010). Nanocellulose, the generally accepted and overused trade name of cellulosic nanoparticles, includes cellulose nanocrystals or whiskers, and cellulose microfibrils or microfibrillated cellulose (MFC). The former are obtained by submitting natural fibers to strong acid hydrolysis followed by a sonication treatment to obtain stiff rod-like nanoparticles. The latter results from multiple mechanical shearing actions performed on natural fibers, this disintegration process allowing release of the constitutive cellulosic microfibrils.

Even if petrochemical based polymers predominate in packaging of foods due to their easy processing, excellent barrier properties and low cost, packaging is one area in which nanocellulosic-reinforced polymeric films can be of interest because of the possibility to produce films with high transparency, and improved mechanical and barrier properties (Azeredo, 2009). Sustainability and green issues continue as top priorities for many businesses and individuals, stimulating the search for non-petroleum based structural materials. Research in this area is burgeoning but it is evolving rapidly to enhance the barrier properties and to overcome certain limitations. In addition, it is well known that molecules penetrate with difficulty in the crystalline domains of cellulose microfibrils. Moreover, the ability of cellulosic nanoparticles to form a dense percolating network held together by strong inter-particles bonds suggests their use as barrier films.

Only few works reporting the barrier properties of cellulosic nanoparticles or related nanocomposites can be found in the literature. The barrier properties of poly(lactic acid) (PLA) films reinforced with bentonite, a layered silicate, or microcrystalline cellulose (MCC) were compared (Petersson & Oksman, 2006). No reduction of the oxygen permeability was observed for the MCC nanocomposite contrarily to bentonite nanocomposite. This poor performance was ascribed to a poor dispersion of the filler. The water vapor transmission rate of cellulose nanocrystals reinforced glycerin plasticized carboxymethyl cellulose (CMC) films was found to decrease slightly upon heat-treatment (Choi & Simonsen, 2006). Transport properties of poly(vinyl alcohol) (PVA) films cross-linked with poly(acrylic acid) (PAA) and reinforced with

* Corresponding author. Present address: Universidade Federal de Rio de Janeiro (UFRJ), Departamento de Engenharia Metalúrgica e de Materiais, Coppe, Rio de Janeiro, Brazil. Tel.: +33 476826995; fax: +33 476826933.
E-mail address: Alain.Dufresne@pagora.grenoble-inp.fr (A. Dufresne).

0144-8617/$ – see front matter © 2010 Elsevier Ltd. All rights reserved.
doi:10.1016/j.carbpol.2010.10.036

cellulose whiskers were studied, including water vapor transport rate and the transport of trichloroethylene (Paralikar, Simonsen, & Lombardi, 2008). Reduced moisture transport was reported upon filler addition and improved performance was obtained for surface carboxylated nanocrystals due to improved dispersion. Cellulose nanoparticles prepared by drop-wise addition of ethanol/HCl aqueous solution into a NaOH/urea/H_2O suspension of MCC were found to decrease the water vapor permeability of glycerol plasticized-starch films (Chang, Jian, Zheng, Yu, & Ma, 2010). Improved water vapor barrier properties of biopolymer films, such as mango puree based edible films (Azeredo et al., 2009) and glycerol plasticized chitosan films (Azeredo et al., 2010) were also reported. It was also found that the use of MFC as surface layer on paper sheet reduced strongly its oxygen permeability (Syverud & Stenius, 2009). It was ascribed to the dense structure formed by the microfibrils resulting in reduced sheet porosity.

The effect of other polysaccharide nanoparticles, such as platelet-like starch nanocrystals, on barrier properties was also investigated. Both the water vapor and oxygen permeability of filled natural rubber films were found to decrease (Angellier, Molina-Boisseau, Lebrun, & Dufresne, 2005). No significant decrease of the water vapor permeability was observed for sorbitol plasticized pullulan films reinforced with starch nanocrystals up to 20 wt% (Kristo & Biliaderis, 2007). For higher filler content enhanced barrier properties were reported.

The aim of the present study was to characterize the transport properties, viz. water vapor and gas (carbon dioxide, nitrogen and oxygen) permeability, of 100% nanocellulose films composed of either cellulose nanocrystals or MFC. The cellulosic nanoparticles were extracted from the same source, i.e. sisal fibers. Although the effect of these nanoparticles on the barrier properties of composite films were studied separately, no comparison between these two nanoparticles has been reported in the literature.

2. Experimental

2.1. Materials

Sisal cellulose whiskers (W) and microfibrillated cellulose (MFC) were prepared from native sisal fibers (*Agave sisalana*) originating from northeast Brazil and purchased in Mariana (Minas Gerais, Brazil).

2.1.1. Cellulose whiskers (W)

Cellulose nanocrystals were prepared as reported elsewhere (Siqueira et al., 2009). Briefly, sisal fibers were cut with a FRITSCH Pulverisette mill, until obtaining fine particulate fibers. These fibers were treated with a 4 wt% NaOH solution at 80 °C for 2 h under mechanical stirring (treatment done in triplicate) to purify cellulose. After each treatment fibers were filtered and washed with distilled water until the alkali was completely eliminated. A subsequent bleaching treatment was carried out at 80 °C for 4 h under mechanical stirring and repeated 4 times to bleach the fibers. The solution used in this treatment consisted of equal parts of acetate buffer, aqueous chlorite (1.7 wt% in water) and distilled water. After each treatment the fibers were filtered and washed with distilled water. Acid hydrolysis was achieved at 50 °C with 65 wt% sulfuric acid (pre-heated) for about 40 min under mechanical stirring. The fiber content during all these chemical treatments was in the range 4–6 wt%. The suspension was diluted with ice cubes to stop the reaction and washed until neutrality by successive centrifugations at 10,000 rpm at 10 °C for 10 min each step and dialyzed against distillated water, in the sequence. Afterwards the sisal whiskers suspension was homogenized by using an Ultra Turax T25 homogenizer for 5 min and filtered using glass filter no. 1. Some drops of chloroform were added to the whiskers suspension which was stored at 4 °C.

2.1.2. Microfibrillated cellulose (MFC)

Sisal MFC was prepared as reported elsewhere (Siqueira, Bras, & Dufresne, 2009). A 2.0 wt% suspension of bleached sisal fibers was pumped through a microfluidizer processor (Model M-110 EH-30). The slurry was passed through the valves that applied a high pressure. Size reduction of products occurs in Interaction Chamber (IXC) using cellules of different sizes (400 μm and 200 μm).

2.1.3. Films preparation

W and MFC films were obtained by water evaporation of sisal cellulose whiskers and MFC suspensions, respectively. The aqueous suspensions were cast in Teflon molds and allowed to evaporate at 25 °C for 5 days. Films, around 20 μm thick, were further dried at 60 °C overnight and conditioned at 25 °C in a desiccator containing P_2O_5 to insure a 0% relative humidity (RH) atmosphere for at least 24 h before testing.

2.2. Characterizations

2.2.1. Morphological investigation

The morphology of W and MFC films was investigated using a ZEISS-ULTRA55 scanning transmission electron microscope with field emission gun (SEM-FEG). The secondary electron detector INLENS SE 1 was located in the GEMINI column. It allows observation with a very low acceleration voltage of 1 kV and avoids degrading sensitive samples such as cellulose keeping a high resolution. The working distance was 5.9 mm and the films were coated with a thin palladium layer (1 nm). The porosity of the films was estimated from air permeability measurements taking MF-millipore membranes having known porosity and presenting the same surface as standard. Measurements were performed using an Akustron from Equintech (Rycolbelgroup).

2.2.2. Transport properties

The transport properties of small molecules through W and MFC films were studied with methods appropriate to the nature of the diffusing molecules. Before each analysis, samples were dried in desiccators under vacuum pressure with P_2O_5. All permeation and sorption measurements were performed at 25 °C.

2.2.2.1. Water sorption. Dynamic gravimetric vapor sorption (DVS) is a well established method for the determination of vapor sorption isotherms. The DVS Advantage 1 instrument (Surface Measurement Systems, London, UK) used for the study measured the uptake and loss of vapor gravimetrically using a recording ultramicrobalance with a mass resolution of ±0.1 μg. The temperature was maintained constant at 25.1 ± 0.1 °C, by enclosing the entire system in a temperature-controlled incubator. For the DVS experiments, W and MFC samples (~10–40 mg) were placed in a quartz sample pan. The sample pan was then placed in the DVS at the desired temperature and dried at 0% RH to establish a dry mass. After reaching a plateau, the dry mass was achieved and the sample was exposed to the following RH profile: 0–5% RH with 2.5% RH increments, 5–20% RH with 5% RH increments, 20–90% RH with 10% increments and finally 95% RH. Mass equilibrium was reached at each humidity level by measuring the percent mass change with respect to time (i.e. slope or dm/dt). Once the mass slope was below a predetermined threshold value and equilibrium was achieved, the experiment proceeded to the next programmed humidity stage. The values of water content at equilibrium were used to build the sorption isotherm. The relationship between water activity a_w (with $a_w = p/p_{sat}$, the ratio of pressure p to saturation vapor pressure p_{sat}) and the equilibrium

moisture content M_{eq} at constant temperature was described by a sorption isotherm. M_{eq} was defined as the ratio of the difference between the mass of the wet sample at equilibrium state (M_w) and dry mass (M_d) to the dry matter mass (Eq. (1)):

$$M_{eq} = \frac{M_w - M_d}{M_d} \quad (1)$$

2.2.2.2. Gas permeation. The carbon dioxide, nitrogen and oxygen permeation measurements were carried out by the "time-lag" method, a variable pressure method (Joly, Le Cerf, Chappey, Langevin, & Muller, 1999; Lixon, Ben Doudou, Chappey, Dargent, & Marais, 2009). The gas permeation cell consisted of two compartments separated by the studied film. A preliminary high vacuum desorption was realized on both sides of the film for at least 1 h. Then, upstream side was provided with gas under test at pressure p_1 = 1 bar.

The pressure increase in the downstream (p_2) was recorded as a function of time with a datametric pressure sensor (PFEIFFER VACUUM, 0–1 mbar). A steady-state line was obtained after a transitory state. The permeability coefficient, P, expressed in barrer units (1 barrer = 10^{-10} cm^3 (STP) cm cm^{-2} s^{-1} cmHg^{-1}) was calculated from the slope of the steady state line (dp/dt) (Eq. (2)):

$$P = \frac{dp}{dt}\frac{L \cdot V}{A \cdot R \cdot T \cdot \Delta p} \quad (2)$$

where $\Delta p = (p_1 - p_2)$ is the pressure difference between the two sides of the film, A the exposed area (11.341 cm^2), L (cm) the thickness of the film, R the ideal gas constant and V the downstream volume (98.13 cm^3).

3. Theoretical background

3.1. Water sorption

3.1.1. Sorption isotherm

Water sorption isotherm equations are useful for predicting water sorption properties of cellulosic materials, and allow providing insight into the interaction between water molecules and cellulosic compounds. Although several mathematical models exist to describe water sorption isotherms of hydrophilic materials, such as cellulosic systems, none of the equations gives accurate results throughout the whole range of water activities, or for all types of materials. Models available in the literature to describe moisture sorption isotherms can be divided into three categories: (1) Rogers classification (Rogers, 1965) for kinetics models based on a mono-layer film, (2) Brunauer, Emmett and Teller (BET) (Brunauer, Emmett, & Teller, 1938) model type I classification concerning kinetics models based on a multilayer and condensed film, and (3) semi-empirical models as Ferro-Fontan, Henderson, Smith, Oswin, Peleg and Halsey models (Al-Muhtaseb, McMinn, & Magee, 2004).

For the water sorption of cellulosic materials, the Park model (Gouanve, Marais, Bessadok, Langevin, & Metayer, 2007) and GAB equation (Bessadok et al., 2009) are usually used to fit the sorption isotherm curve. The adsorption models, such as BET and GAB models (Brunauer et al., 1938), consider that water molecules condense layer by layer on adsorption surfaces (external surfaces of specific sites or internal surfaces of micro-pores/cavities for instance). These models need two parameters to be defined, namely the amount of water C_m corresponding to one monolayer and the constant K_{ads} linked to the adsorption enthalpy difference between the first layer and the following (Eq. (3)). For instance, the BET model was used to determine the amount of moisture adsorbed as a monomolecular layer at the surface of lyocell and cotton fibers (Okubayashi, Grissier, & Betchold, 2004). The GAB model was used to fit the sorption isotherm data in cassava starch films (Mali, Sakanaka, Yamashita, & Grossmann, 2005).

$$C = C_m \frac{C_G K_{ads} \cdot a_w}{(1 - K_{ads} a_w) \cdot (1 + C_G - 1)} \quad (3)$$

where C_G is the Guggenheim constant.

The Park model [$C = f(a_w)$, Eq. (4)] involves three terms (Gouanve et al., 2007; Guggenheim, 1966). The first one describes the Langmuir sorption which leads to a plateau of concentration when the water activity increases, corresponding to the saturation of the specific sites of sorption. The second term gives a water concentration that increases linearly with the water activity (Henry's law). Finally, the third term is a power function which represents the aggregation phenomenon (water clustering) at high activity. The specific sites of sorption can be ions, polar groups, micro-cavities or micro-porosities, and are often considered as the nuclei of the water aggregates. As suggested by Morton and Hearle (1997) water molecules adsorb directly on cellulose hydroxyl groups from the external surface, amorphous regions, inner surface of voids and crystallites. Additional water molecules can adsorb on the water molecules binding the fiber directly.

$$C = \frac{A_L \cdot b_L \cdot a_w}{1 + b_L \cdot a_w} + K_H \cdot a_w + K_a \cdot n \cdot a_w^n \quad (4)$$

where A_L is the Langmuir capacity constant, b_L the Langmuir affinity constant, K_H the Henry's solubility coefficient, K_a the equilibrium constant for the clustering reaction, and n the average number of water molecules per cluster.

To evaluate the validity of the fit by the model used, the mean relative percentage deviation modulus (E) can be calculated (Eq. (5)). This procedure is widely adopted throughout the literature, and a modulus value below 10% usually reveals a good fit (Lomauro, Bakshi, & Labuza, 1985).

$$E = \frac{100}{N}\sum_{i=1}^{N}\frac{|m_i - m_{pi}|}{m_i} \quad (5)$$

m_i being the experimental mass, m_{pi} the calculated mass with the model, and N the number of experimental data.

3.1.2. Sorption kinetics

A change of water vapor activity (from a_{wi} to $a_{w(i+1)}$) induces a variation of the water content of the sample with time until a new equilibrium is reached. The analysis of this sorption kinetics allows the calculation of the diffusivity of water in the material assuming some hypotheses. In this work, cellulosic materials were treated as dense and homogeneous materials while the transport phenomena were assumed to be governed by a solution-diffusion model relative to the transport of small molecules in polymers. Considering the usual boundary conditions for gas and vapor sorption measurements, Fick's laws lead to the determination of two diffusion coefficient D_1 and D_2 (Eqs. (6) and (7)):

$$Q_t = k_1 \cdot \sqrt{t} \Rightarrow D_1 = \frac{k_1 \cdot \pi \cdot L^2}{16} \quad (6)$$

$$\ln(1 - Q_t) = k_2 t + b_2 \Rightarrow D_2 = \frac{k_2 \cdot L^2}{\pi^2} \quad (7)$$

where D_1 and D_2 are the first half- and second half-sorption coefficients, respectively, and k_1 and k_2 are the coefficients corresponding to the first half- and second half-sorption coefficients, respectively.

3.1.3. PEK's model

It has been found that the sorption and desorption kinetics for each RH level can be well predicted assuming two parallel, inde-

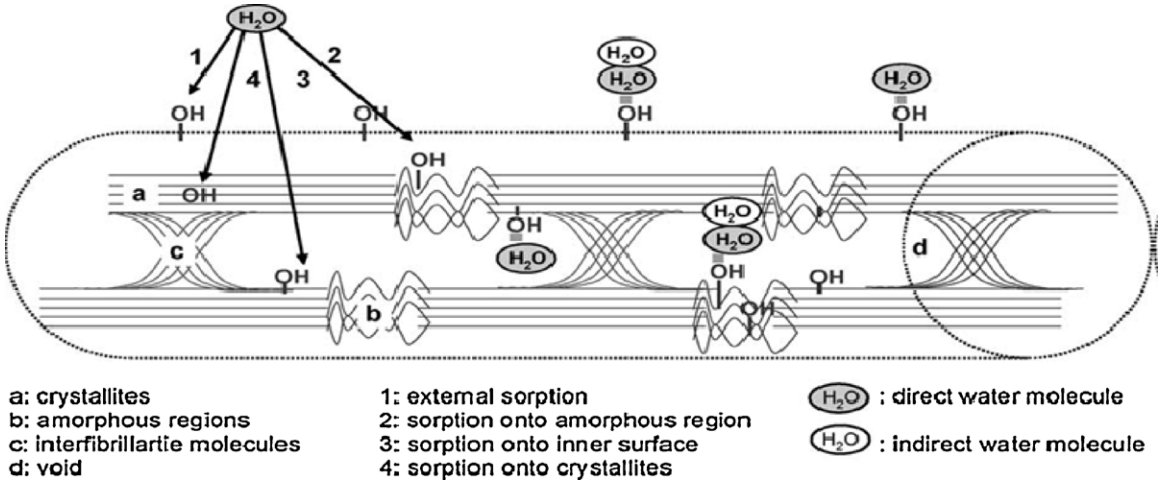

Fig. 1. A schematic diagram of direct and indirect moisture sorption onto external surface (1), amorphous regions (2), inner surface of voids (3), and crystallites (4) (Okubayashi et al., 2004).

pendent first order processes. Indeed, Kohler, Alex, Brielmann, and Ausperger (2006) and Okubayashi et al. (2004) reported that water exchange of natural fibers such as flax and hemp can be modeled by two parallel independent first order processes. It was defined as the "Parallel Exponential Kinetics" model (PEK-model). The model offers two different mechanisms for the exchange of water vapor related to different sorption sites. According to this method, experimental data of the moisture content can be simulated as a function of time using Eqs. (8) and (9).

For the sorption $M_t = M_1(1 - e^{-t/\tau_1}) + M_2(1 - e^{-t/\tau_2})$ (8)

For the desorption $M_t = -M_1(1 - e^{-t/\tau_1}) - M_2(1 - e^{-t/\tau_2})$ (9)

where M_t is the mass at any time t, M_1 and M_2 correspond to the masses at equilibrium state, and τ_1 and τ_2 are characteristic times to obtain M_1 and M_2, respectively.

It is considered that $\tau_1 + \tau_2$ is the time necessary to reach 63% of M_{1+2} (Eq. (10))

$$M_t = M_{1+2}(1 - e^{-1}) = M_{1+2} \times 0.63 \quad (10)$$

Subscripts 1 and 2 refer to the two kinetic processes defined for fast and slow sorption sites, respectively. The fast and slow sorption sites can be related to different types of amorphous regions, external/internal fiber surfaces and direct/indirect sorption (Morton & Hearle, 1997) as shown in Fig. 1. Water molecules adsorb directly on the hydroxyl groups of the external surface, amorphous regions, inner surface of voids and crystallites. Additional water molecules can adsorb on the water molecules binding the fiber directly. The direct sorption of the water molecules onto the external surface and amorphous regions is fast while the indirect sorption onto the inner surface and crystallites is relatively slow.

These equations have been used to fit experimental data. In this way, PEK parameters M_1 and M_2 were calculated for at each moisture interval. The fit shows outstanding correlation factors of $R^2 > 0.99$.

3.2. Gas permeation

For gas permeation and assuming no specific interaction between gas and polymer, the diffusion coefficient can be assumed to be constant. Usually, its value can be calculated from the time-lag t_L using Eq. (11).

$$D = \frac{L^2}{6t_L} \quad (11)$$

L being the film thickness and D the diffusion coefficient. The solubility coefficient S is then deduced from the ratio P/D (Cussler, 1997). Finally, the fundamental parameters characterizing the film separation performance are the permeability coefficient, P, and the ideal selectivity, $\alpha_{A/B}$. The ideal gas selectivity is the ratio of the permeability coefficient of two gases A and B (Eq. (12)) (Freeman, 1999):

$$\alpha_{A/B} = \frac{P_A}{P_B} = \frac{D_A S_A}{D_B S_B} \quad (12)$$

where P_A and P_B are the permeabilities of the more and less permeable gas, respectively.

4. Results and discussion

4.1. Morphological analyses

Transmission electron microscopy (TEM) observations of sisal cellulose whiskers reported in our earlier study (Siqueira et al., 2009) show that these nanoparticles occur as straight rod-like nanoparticles. Their length and diameter were determined by using digital image analysis (ImageJ) and values of 215 ± 67 nm and 5 ± 1.5 nm, respectively, were reported. From scanning electron microscopy (SEM) analysis of sisal MFC (Siqueira et al., 2009), a web-like structure was observed and it was found that the average diameter was 52 ± 15 nm showing that mostly microfibrils bundles were obtained. It was not possible to determine the length of the microfibrils.

Fig. 2 shows SEM-FEG observations of the surface of W (panel a) and MFC films (panel b). Both films display a porous structure similar to a paper sheet. The rod-like and web-like morphology of sisal whiskers and MFC, respectively, is clearly observed from these microscopic observations. Moreover, microfibril bundles are seen in Fig. 2b. The W film consists of a mat of H-bonded cellulosic whiskers whereas the MFC film seems to consist of trapped filaments. Residual lignin, extractive substances and fatty acids present at the surface of MFC (Bendahou, Kaddami, & Dufresne, 2010; Dufresne, Cavaillé, & Vignon, 1997) are supposed to constitute the binding agent between microfibrils. These differences were evidenced from porosity measurements which were found around 62% and 35% for W and MFC films, respectively. The higher porosity of the W film results in a lower density ($0.9\,g\,cm^{-3}$) compared to the MFC film ($1.33\,g\,cm^{-3}$).

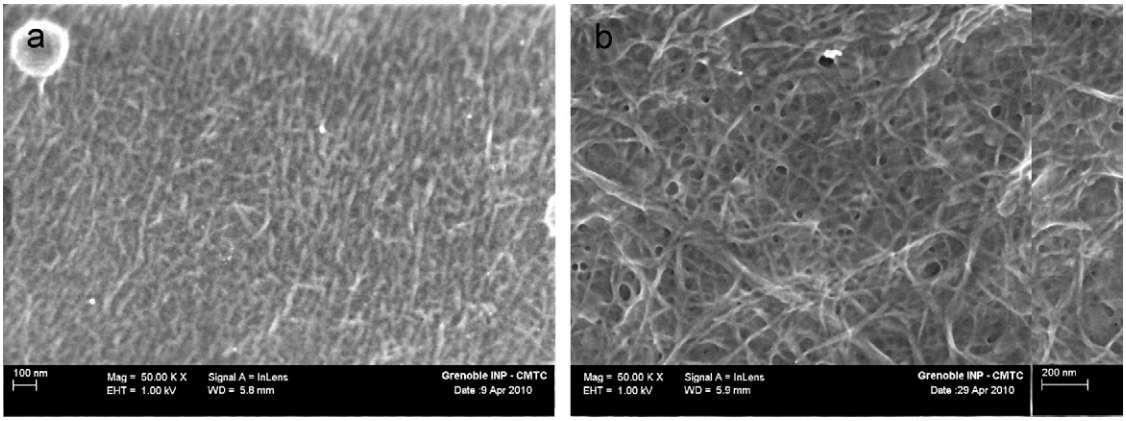

Fig. 2. Scanning electron micrographs (SEM-FEG) of a film of (a) sisal cellulose whiskers and (b) sisal MFC.

4.2. Water sorption

4.2.1. Sorption isotherm

From water sorption kinetics performed on W and MFC films, the water sorption isotherm curves were deduced and are shown in Fig. 3. Both curves display a sigmoid or S-shape profile. This typical curve shape is classically obtained for cellulosic based materials and can be generalized to many hydrophilic materials (Gocho, Shimizu, Tanioka, Chou, & Nakajima, 2000).

As observed in Fig. 3, the W film absorbed as much water as the MFC film, which was surprising because of the structural difference (morphology, degree of crystallinity, polarity...) between both kinds of nanoparticle. A very good repeatability of the measurements was obtained (Fig. 4). However, it is worth noting that both materials are mainly composed of α-cellulose (around 75 ± 2%), which plays an important role in the water sorption uptake. To have a better approach of this water sorption behavior, a sorption–desorption–sorption cycle has been achieved on each sample. The ensuing isotherms are shown in Fig. 4. As can be seen, these systems are completely reversible and repeatable.

In order to describe the water sorption behavior of sisal W and MFC films, the GAB and Park models were used to fit the isotherm curves according to Eqs. (3) and (4), respectively. The different parameters of these models for cellulosic samples are given in Tables 1 and 2, respectively. From the E values, it appears that the Park model gives the best fit compared to the GAB equation. The examination of the fitting data (regression coefficient R^2, deviation modulus E) seems to indicate that the Park model is consistent with the experimental data and well

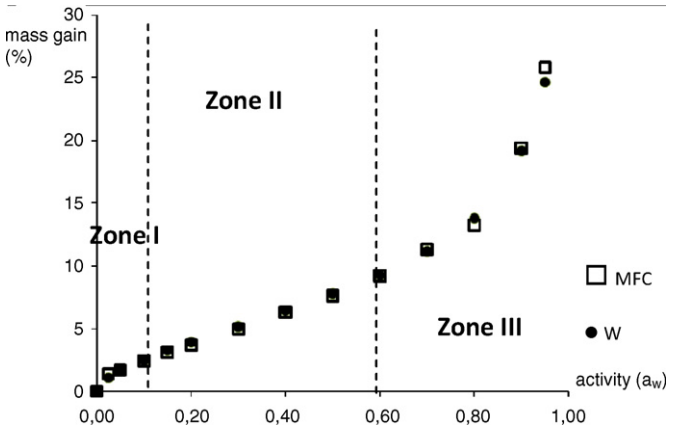

Fig. 3. Water sorption isotherms for W and MFC films measured at 25 °C.

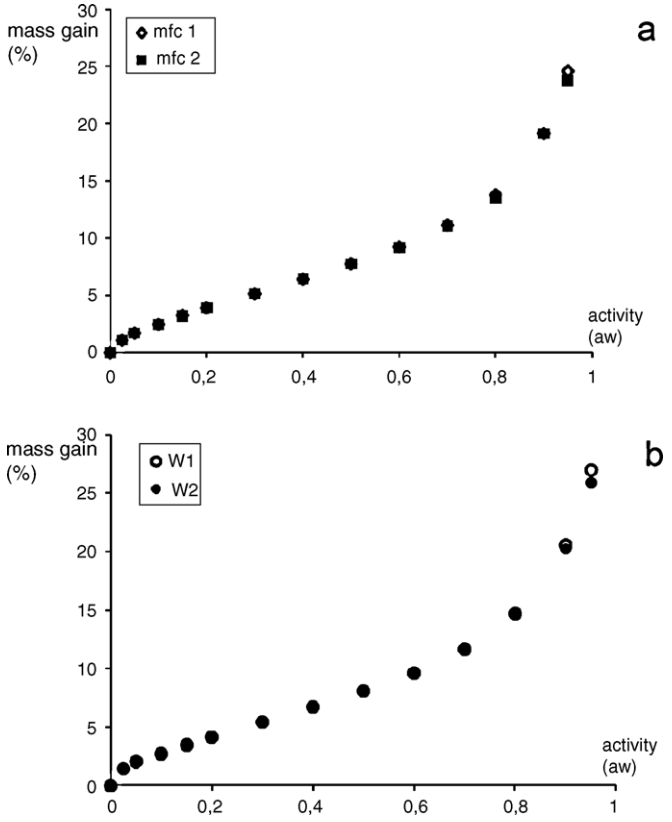

Fig. 4. Water vapor sorption at 25 °C for (a) W and (b) MFC films where only the sorption is represented (cycle 1: sorption–desorption; cycle 2: sorption).

Table 1
Sorption parameters of the Park model (Eq. (4)) determined from water sorption isotherms for W and MFC films.

	A_L	b_L	K_H	K_a	n	E (%)
W	1.4	230	13.7	21.1	10	6.5
MFC	1.0	200	13.7	18.2	11	1.2

Table 2
Sorption parameters of the GAB model (Eq. (3)) determined from water sorption isotherms for W and MFC films.

	C_m	K_{ads}	C_G	E (%)
W	5.1	0.8	8.8	7.6
MFC	9.8	0.8	5.1	3.1

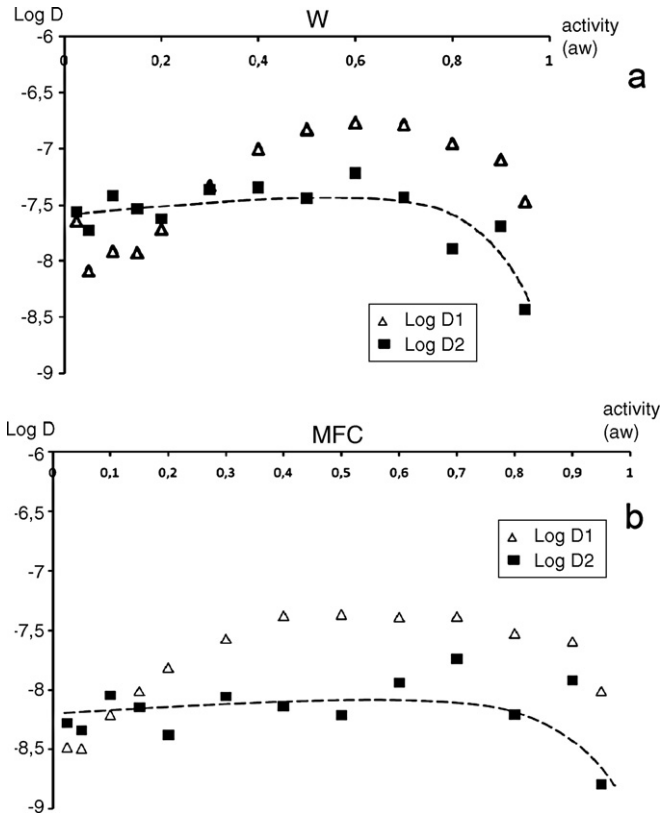

Fig. 5. Water vapor sorption at 25 °C in (a) W and (b) MFC films: evolution of D_1 and D_2 as a function of the relative humidity.

describes the water sorption isotherms in the whole water activity range.

Each parameter of the Park model has a predominant effect in a limited water activity range. Langmuir's terms, A_L (Langmuir capacity constant) and b_L (Langmuir affinity constant) have an influence in zone I at lower water activity ($a_w < 0.1$). Henry's solubility coefficient, K_H, defines the slope of the isotherm in zone II ($0.1 < a_w < 0.6$). The values K_a (equilibrium constant for the clustering reaction) and n (average number of water molecules per cluster) are linked to the equilibrium state corresponding to the aggregate formation in zone III ($a_w > 0.6$) (Fig. 3). From the analysis of the model parameters, we can notice that both W and MFC films have nearly the same constant values.

4.2.2. Sorption kinetics (diffusion coefficient)

The diffusion coefficients (D_1 and D_2) were determined for W and MFC films from sorption kinetics according to Eqs. (6) and (7), respectively. The evolution of D_1 and D_2 as a function of a_w in the semi-logarithmic scale $\log(D) = f(a_w)$ is shown in Fig. 5. It appears that D_1 and D_2 depend appreciably on the water activity. As show in Fig. 5, the values of both diffusion coefficients (D_1 and D_2) are higher for cellulosic W film than for MFC. This result is quite surprising assuming that W structure is more organized (higher crystallinity) than that of MFC. It should lead to lower diffusion coefficients for the former film. The presence of residual lignin, extractive substances and fatty acids at the surface of MFC promoting higher hydrophobicity of the film (Bendahou et al., 2010) could explain this result. This difference in the surface chemistry of both sisal nanoparticles was well evidenced from contact angle measurements, W and MFC films displaying water contact angles of 44.6° and 59.4°, respectively (Siqueira, Bras, & Dufresne, 2010).

For each specimen, it is observed that D_1 first decreases for very low water activities ($a_w < 0.1$). It can be explained by the fact that water molecules could exert an antiplasticizing effect on diffusion. Water molecules interact with polar groups from the surface of the nanoparticles leading to hydrogen bonds that increase the cohesion between cellulosic chains thus reducing the water mobility. A similar phenomenon was reported for cereal-based products (Marzec & Lewicki, 2006) and low content glycerol plasticized tapioca starch films (Chang, Karim, & Seow, 2006). The 'water antiplasticizing range' appeared to become increasingly narrow with an increase in moisture content until the antiplasticizing effect was no longer evident and water reverted to its typical role of plasticizer for $a_w > 0.1$. For water activity ranging between 0.1 and 0.5, the increase of the diffusion coefficients was due to the plasticization of the material by water (swelling effect) while for higher water activity ($a_w > 0.5$) the decrease of D_1 and D_2 was due to water molecules clustering (Gouanve et al., 2007). This was indicative of a water sorption mechanism complying with the Park model. Part of the water was adsorbed on specific sites (low mobility of the fixed water molecules) and the rest dissolved according to Henry's process (higher mobility of the dissolved molecules) later forming aggregates at high water activity (low mobility of the aggregates).

However, other effects have to be considered. The sorption kinetics was studied according to successive steps with limited activity increments Δa_w and, for each step, the value of D_2 was found to be clearly lower than D_1. Generally, D_2 values were higher than D_1 values due to the swelling effect during the sorption (Gouanve et al., 2007). In our case, D_2 values are lower for a wide range of activity. The D_2 values (second half-sorption coefficient) should be more representative of the diffusion of water in the core of the nanofiber while D_1 (first half-sorption coefficient) should be more characteristic of the diffusion through the surface. This unusual effect indicates heterogeneity of the nanofibers which could affect the plasticization effect. It seems that during the sorption kinetic instead of having an increase of the water diffusivity a barrier effect due to the presence of water at the surface occurs.

Indeed, this atypical behavior with $D_2 < D_1$ might be a result of a structuring effect of water during the water sorption in the material. During sorption kinetics, it seems that molecule penetration becomes more and more difficult in the material due to a strong cohesion between the chains (structural reorganization). In that way, the diffusion of water is rather governed by the surface effect than by the core of the swelling material, so that the water diffusivity is reduced during the sorption process. The ability of the chains to form hydrogen bonds, the crystallinity, the structure orientation, the material geometry etc. are major factors which affect the diffusion. These parameters have to be analyzed in order to understand the phenomena encountered here.

4.3. PEK's model

From a kinetic point of view, it is well-know that mechanisms of moisture sorption in hydrophilic fiber materials, e.g. cellulosic fibers, are comparatively complex because it involves a continuous change of the structure of the fiber owing to swelling (Okubayashi et al., 2004). In this case, another approach of the diffusion mechanisms was developed by following sorption and adsorption kinetics on each level of relative humidity. Indeed, Kohler et al. (2006) and Okubayashi et al. (2004) have reported that water exchange in natural fibers such as flax and hemp can be modeled by two parallel independent first order processes, which was defined here as the "Parallel Exponential Kinetics" model (PEK-model). The model offered two different mechanisms for the exchange of water vapor

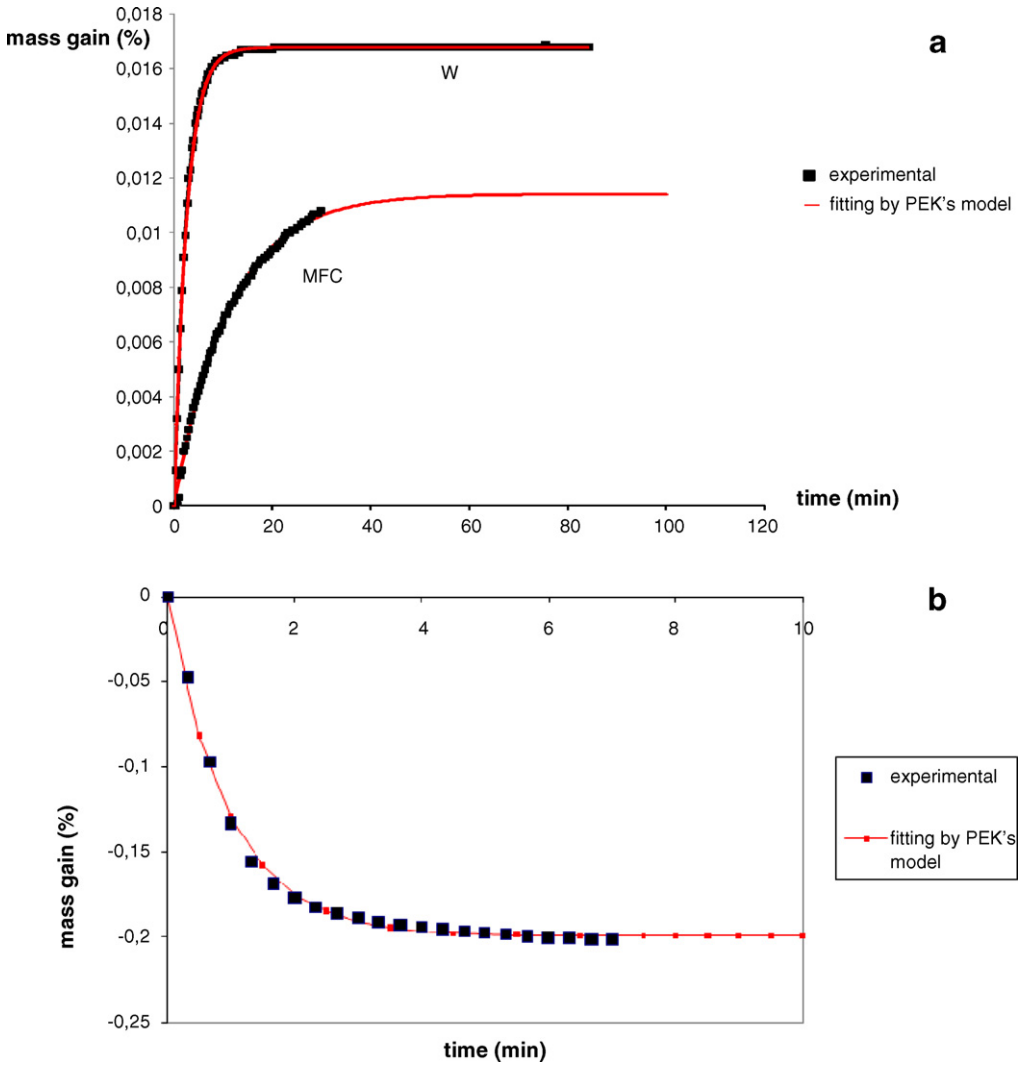

Fig. 6. Example of PEK's simulations for experimental data of (a) moisture regain for $a_w = 0.1–0.2$ ($R^2 > 0.99$), and (b) loss for W and MFC films for $a = 0.95–1$ ($R^2 > 0.99$) at 25 °C. Results of the simulation are shown in solid lines.

relating to different sorption sites. According to this method, experimental data of the moisture content was simulated as a function of time. A result of the simulation for sisal cellulose W and MFC films is shown in Fig. 6 using the general equation of the PEK's model, Eq. (13) and (14).

$$\text{Sorption}: \quad M_t = M_{1+2}(1 - e^{-t/(\tau_1+\tau_2)}) \tag{13}$$

$$\text{Desorption}: \quad M_t = -M_{1+2}(1 - e^{-t/(\tau_1+\tau_2)}) \tag{14}$$

where M_t is the mass change at any time t, M_1 and M_2 are the mass at equilibrium state, τ_1 and τ_2 are the characteristic times for which M_1 and M_2 are reached, respectively, and M_{1+2} corresponds to the sum of M_1 and M_2.

The predicted curves show a good agreement with experimental data, suggesting that the PEK model is an appropriate model to describe the water sorption in sisal nanocellulosic materials. Generally, with any sorption kinetics the structure and size of the sample have to be taken into account. Particularly during sorption processes, physical sample structure (fiber, yarn and fabric) could influence the final result, so that in this study the same mass of fibrous materials with similar physical structure (diameter and length) were selected.

The PEK parameters, M_1 and M_2 were calculated for low ($a_w \leq 0.5$) and high activities ($a_w > 0.5$) (Table 3). As can be seen, the components of fast sorption dominated over that of slow sorption process ($\tau_1 > \tau_2$ and $M_1 > M_2$) especially at lower RH ($a_w < 0.5$). This suggests that water molecules predominantly adsorb directly on the external surfaces and on the low-ordered amorphous regions. Less moisture penetrates into internal surfaces and in high-ordered amorphous regions at low RH (Okubayashi et al., 2004). Both cel-

Table 3
PEK's model parameters: M_1, M_2, τ_1 and τ_2 values, corresponding to fast (1) and low (2) kinetics, respectively, for low ($a_w = 0.10–0.20$) and high water activity ($a_w = 0.95–1$), determined at 25 °C for W and MFC films.

	Low activity ($a_w = 0.1–0.2$)				High activity ($a_w = 0.95–1$)			
	M_1($\times 10^3$ g)	τ_1 (s)	M_2($\times 10^4$ g)	τ_2 (s)	M_1($\times 10^4$ g)	τ_1 (s)	M_2($\times 10^3$ g)	τ_2 (s)
W	6	16.4	2	0.017	1	0.5	49	19.2
MFC	18	47.2	8.6	0.005	100	1.5	112	27.4

Table 4
Permeability coefficient (P), diffusion coefficient (D), and solubility (S) of N_2, CO_2, O_2 for W and MFC films measured at 25 °C, 1 bar.

	Samples	P (barrer)[a]	$D(\times 10^8$ cm^2/s)	$S(\times 10^3$ cm^3 STP cm^{-3} cmHg^{-1})
CO_2	W	118.8 ± 1.2	21.7 ± 0.7	54.9 ± 1.6
	MFC	0.100 ± 0.002	0.040 ± 0.001	25.9 ± 0.7
N_2	W	161.7 ± 3.2	51.2 ± 1.5	31.3 ± 0.9
	MFC	0.150 ± 0.004	0.0100 ± 0.0001	12.3 ± 0.4
O_2	W	140.7 ± 2.7	79.5 ± 2.4	17.7 ± 0.5
	MFC	0.090 ± 0.001	0.00280 ± 0.00001	30.8 ± 1.0

[a] 1 barrer = 10^{-10} cm^3 (STP) cm cm^{-2} s^{-1} cmHg^{-1}. N.B: cm^3 (STP) is the amount of gas in cm^3 at standard temperature and pressure (273 K, 1 bar).

lulosic films (W and MFC) display a similar tendency. These results are in agreement with diffusion coefficient variations D_1 and D_2. Indeed, D_2 values were found to be higher than D_1 values at low water activity. The former should be more representative of the diffusion of water in the core of the fiber while D_1 should be more characteristic of the diffusion at the surface.

As reported in Table 3, the component of slow sorption dominated over that of fast sorption process ($\tau_1 < \tau_2$ and $M_1 < M_2$) at higher RH ($a_w > 0.5$). It seems that all external sites were already occupied. Also, water molecules can be only sorbed inside the sample. These results agree with the variation of the diffusion coefficients D_1 and D_2. D_1 was found higher than D_2 at water activity $a_w > 0.3$. The fact that at high relative humidity, the slow sorption mechanism is predominant is consistent with the presence of water clusters.

PEK's model can be applied, considering two different mechanisms for the exchange of water vapor relating to slow and fast sorption sites and to different sorption sites. This result should be taken with care because this model is only phenomenological and gave a very simplify draw of the real system.

4.4. Gas permeation

The carbon dioxide, nitrogen and oxygen permeation results are gathered in Table 4. Experiments have been performed at 2.013×10^{-5} Pa (constant pressure) because of the low mechanical resistance of the samples (Siqueira et al., 2009), at a constant temperature (room temperature) and with the same vacuum time (1 h).

Usually, gas permeability coefficient of polymers should follow this order: $P_{N_2} < P_{O_2} < P_{CO_2}$ (Van Krevelen, 1997) and $D_{CO_2} \sim D_{N_2} < D_{O_2}$ (Lebrun, Bruzaud, Grohens, & Langevin, 2006) in accordance with the decrease of the diameter of the molecules ($d_{CO_2} = 0.39 \times 10^{-2}$ nm$\sim d_{N_2} = 0.38 \times 10^{-2}$ nm $> d_{O_2} = 0.35 \times 10^{-2}$ nm) (Kumins & Kwei, 1968). However, it can be noted that the variation of the gas permeability should depend on the kinetic diameter (different from the size) of the gas which varies according to: $d_{CO_2} = 0.33\,\text{nm} < d_{O_2} = 0.346\,\text{nm} < d_{N_2} = 0.364\,\text{nm}$. As can be seen from values reported in Table 4, this tendency is observed for the permeability coefficients measured for the W film but not for MFC. Also, the W film shows significantly higher permeability coefficients than that of MFC, which is surprising considering that cellulose whiskers display a more ordered structure than MFC. The permeability of the W film is more than one thousand times higher than the one of the MFC film, regardless the nature of the gas.

Table 5
Selectivity values (α) for W and MFC films and for N_2, CO_2 and O_2.

α	W	MFC
N_2/CO_2	1.4	1.5
O_2/CO_2	1.2	0.9
N_2/O_2	1.1	1.7

The permeability of a polymer to a penetrating gas depends on both the solubility and the diffusivity. The gas should be first dissolved inside the polymer before diffusing. The solubility and the permeability depend on the boiling point T_b and on the critical temperature T_c of the penetrating gas. The higher the T_b, the higher the condensability and the higher the solubility are. Thus, the $S_{CO_2} > S_{O_2} > S_{N_2}$ ranking should follow the same order as T_c and T_b ($T_{c\,O_2} = -118\,°C > T_{c\,N_2} = -147\,°C$ (except for CO_2 $T_{c\,CO_2} = 31\,°C$) and $T_{b\,O_2} = -183\,°C > T_{b\,N_2} = -195\,°C$ (except for CO_2 $T_{b\,CO_2} = -57\,°C$)).

It is worth noting that the values of the solubility coefficients are in the same order of magnitude for W and MFC films, but not the diffusivity coefficients ones. It could be supposed that these results depend not only on the chemical composition but also on the structural organization too. It might be suggested that gas molecules penetrate more slowly in the MFC film than in the W film probably due to a longer diffusion path as schematized in Fig. 7. Indeed from Table 4, the diffusion coefficient values for MFC are very low (10^{-10} to 10^{-11} cm^2/s) in comparison with those reported for W (10^{-6} to 10^{-7} cm^2/s), around three orders of magnitude. Despite the presence of predominant crystalline structures for W, the lower aspect ratio and the lower packing of the particles (see Fig. 2) in films characterized by a large extent of porosity (Siqueira et al., 2009) would explain the increased mobility of gas molecules in comparison with the MFC structure in which the entangled zones are mainly composed of semi-crystalline fibers of high aspect ratio representing barrier domains that lead to increase the tortuosity of the diffusion pathway.

The selectivity value α, which is a ratio of permeability coefficients, depends on the solubility and size of the diffusing molecules (values given in Table 5). A material is regarded as selective when α is higher than 10. No significant differences for α were observed between W and MFC films. Both present low selectivity. This result should be taken with care because tested films were very thin and brittle.

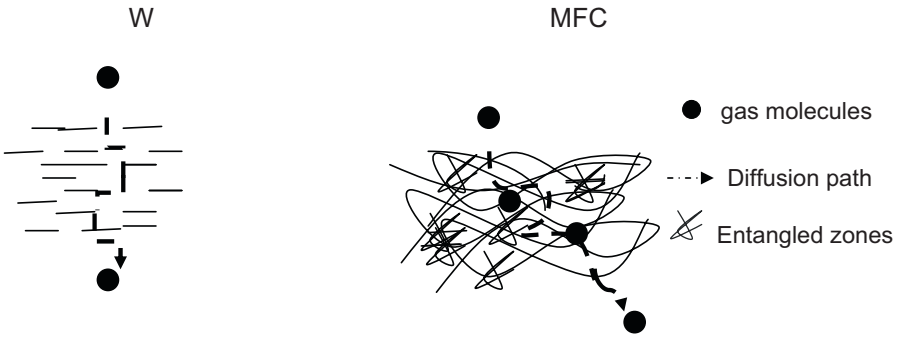

Fig. 7. Schematic representation of the gas molecule diffusivity in W and MFC films.

5. Conclusions

Cellulosic nanoparticles, viz. whiskers and microfibrils, were prepared from sisal fibers and used to obtain transparent films. The transport properties of these films were characterized in detail. Similar water sorption isotherms were observed for both films. The experimental data were well fitted using a Park model. It was found that the water diffusion coefficients were higher for whiskers based films than for MFC. A possible explanation is the presence of residual lignin, extractive substances and fatty acids at the surface of MFC. An unusual behavior was reported for both nanocellulosic films. It was observed that the first half-sorption diffusion coefficient corresponding to the diffusion of water through the surface of the nanoparticles was higher than the second half-sorption diffusion coefficient more representative of the diffusion in the core. It is an indication that the diffusion of water is rather controlled by the surface than by the core, probably because of a barrier effect related to the presence of water at the surface during the sorption kinetics. The PEK's model successfully predicted the water sorption kinetics. The film of sisal cellulose whiskers was found to be much more permeable to gases (by more than thousand times) than MFC despite similar solubility coefficient values. It was suspected that gas molecules penetrate much more slowly in the MFC film because of a longer diffusion path. In addition to a different surface chemistry, it was supposed that entanglements of these long flexible nanoparticles and lower porosity of the films represent barrier domains leading to increased tortuosity of the diffusion pathway. It is now of interest to know if these differences persist when the nanoparticles are embedded within a polymeric matrix. The barrier properties of nanocomposite films obtained from polycaprolactone reinforced with sisal cellulose whiskers and MFC are under investigation and results will be published shortly.

Acknowledgments

The authors gratefully acknowledge ALBAN Program for the financial support (PhD fellowship of G.S.).

References

Al-Muhtaseb, A. H., McMinn, W. A. M., & Magee, T. R. A. (2004). Water sorption isotherms of starch powders – Part 1: Mathematical description of experimental data. *Journal of Food Engineering*, *61*(3), 297–307.

Angellier, H., Molina-Boisseau, S., Lebrun, L., & Dufresne, A. (2005). Processing and structural properties of waxy maize starch nanocrystals reinforced natural rubber. *Macromolecules*, *38*(9), 3783–3792.

Azeredo, H. M., Mattoso, L. H. C., Avena-Bustillos, R. J., Filho, G. C., Munford, M. L., Wood, D., et al. (2010). Nanocellulose reinforced chitosan composite films as affected by nanofiller loading and plasticizer content. *Journal of Food Science*, *75*(1), N1–N7.

Azeredo, H. M., Mattoso, L. H. C., Wood, D., Williams, T. G., Avena-Bustillos, R. J., & McHugh, T. H. (2009). Nanocomposite edible films from mango puree reinforced with cellulose nanofibers. *Journal of Food Science*, *74*(5), N31–N35.

Azeredo, M. C. (2009). Nanocomposites for food packaging applications. *Food Research International*, *42*(9), 1240–1253.

Azizi Samir, M. A. S., Alloin, F., & Dufresne, A. (2005). A review of recent research into cellulosic whiskers, their properties and their application in nanocomposite field. *Biomacromolecules*, *6*(2), 612–626.

Bendahou, A., Kaddami, H., & Dufresne, A. (2010). Investigation on the effect of cellulosic nanoparticles' morphology on the properties of natural rubber based nanocomposites. *European Polymer Journal*, *46*(4), 609–620.

Bessadok, A., Langevin, D., Gouanvé, F., Chappey, C., Roudesli, S., & Marais, S. (2009). Study of water sorption on modified Agave fibers. *Carbohydrate Polymers*, *76*(1), 74–85.

Brunauer, S., Emmett, P. H., & Teller, E. (1938). Adsorption of gases in multimolecular layers. *Journal of the American Chemical Society*, *60*(2), 309–319.

Chang, P. R., Jian, R., Zheng, P., Yu, J., & Ma, X. (2010). Preparation and properties of glycerol plasticized-starch (GPS)/cellulose nanoparticle (CN) composites. *Carbohydrate Polymers*, *79*(2), 301–305.

Chang, Y. P., Karim, A. A., & Seow, C. C. (2006). Interactive plasticizing–antiplasticizing effects of water and glycerol on the tensile properties of tapioca starch films. *Food Hydrocolloids*, *20*(1), 1–8.

Choi, Y. J., & Simonsen, J. (2006). Cellulose nanocrystal-filled carboxymethyl cellulose nanocomposites. *Journal of Nanoscience and Nanotechnology*, *6*(3), 633–639.

Cussler, E. L. (1997). *Diffusion mass transfer in fluid systems*. Cambridge University Press.

Dufresne, A. (2006). Comparing the mechanical properties of high performances polymer nanocomposites from biological sources. *Journal of Nanoscience and Nanotechnology*, *6*(2), 322–330.

Dufresne, A., Cavaillé, J. Y., & Vignon, M. R. (1997). Mechanical behavior of sugar beet cellulose microfibrils. *Journal of Applied Polymer Science*, *64*(6), 1185–1194.

Freeman, B. D. (1999). Basis of permeability/selectivity tradeoff relations in polymeric gas separation membrane. *Macromolecules*, *32*(2), 375–380.

Gocho, H., Shimizu, H., Tanioka, A., Chou, T. J., & Nakajima, T. (2000). Effect of polymer chain end on sorption isotherm of water by chitosan. *Carbohydrate Polymers*, *41*(1), 87–90.

Gouanve, F., Marais, S., Bessadok, A., Langevin, D., & Metayer, M. (2007). Kinetics of water sorption in flax and PET fibers. *European Polymer Journal*, *43*(2), 586–598.

Guggenheim, E. A. (1966). *Application of statistical mechanics*. Oxford, UK: Clarendon Press.

Hubbe, M. A., Rojas, O. J., Lucia, L. A., & Sain, M. (2008). Cellulosic nanocomposites: A review. *BioResources*, *3*(3), 929–980.

Joly, C., Le Cerf, D., Chappey, C., Langevin, D., & Muller, G. (1999). Residual solvent effect on the permeation properties of fluorinated polyimide films. *Separation and Purification Technology*, *16*(1), 47–54.

Kohler, R., Alex, R., Brielmann, R., & Ausperger, B. (2006). A new kinetic model for water sorption isotherms of cellulosic materials. *Macromolecular Symposia*, *244*(1), 89–96.

Kristo, E., & Biliaderis, C. G. (2007). Physical properties of starch nanocrystal-reinforced pullulan films. *Carbohydrate Polymers*, *68*(1), 146–158.

Kumins, C. A., & Kwei, T. K. (1968). In J. Crank, & G. S. Park (Eds.), *Diffusion in polymers*. New York: Academic Press.

Lebrun, L., Bruzaud, S., Grohens, Y., & Langevin, D. (2006). Elaboration and characterisation of PDMS-HTiNbO$_5$ nanocomposite membranes. *European Polymer Journal*, *42*(9), 1975–1985.

Lixon, C., Ben Doudou, B., Chappey, C., Dargent, E., & Marais, S. (2009). Permeation properties of poly(m-xylene adipamide) membranes. *The Journal of Physical Chemistry B*, *113*(11), 3445–3452.

Lomauro, C. J., Bakshi, A. S., & Labuza, T. P. (1985). Evaluation of food moisture sorption isotherm equations 1. Fruit, vegetable and meat-products. *Lebensmittel Wissenschaft & Technologie*, *18*, 111–117.

Marzec, A., & Lewicki, P. P. (2006). Antiplasticization of cereal-based products by water. Part I. Extruded flat bread. *Journal of Food Engineering*, *73*, 1–8.

Mali, S., Sakanaka, L. S., Yamashita, F., & Grossmann, M. V. E. (2005). Water sorption and mechanical properties of cassava starch films and their relation to plasticizing effect. *Carbohydrate Polymers*, *60*(3), 283–289.

Morton, W. E., & Hearle, J. W. S. (1997). *Physical properties of textile fibers*. UK: The Textile Institute.

Okubayashi, S., Grissier, U. J., & Betchold, T. (2004). A kinetic study of moisture and desorption on lyocell fibers. *Carbohydrate Polymers*, *58*(3), 293–299.

Paralikar, S. A., Simonsen, J., & Lombardi, J. (2008). Poly(vinyl alcohol)/cellulose nanocrystal barrier membranes. *Journal of Membrane Science*, *320*(1–2), 248–258.

Petersson, L., & Oksman, K. (2006). Biopolymer based nanocomposites: Comparing layered silicates and microcrystalline cellulose as nanoreinforcement. *Composites Science and Technology*, *66*(13), 2187–2196.

Rogers, C. E. (1965). D. Fox, M. M. Labes, & A. Weissberger (Eds.), *Physics and chemistry of the organic solid state*. New York: John Wiley & Sons Inc.

Siqueira, G., Bras, J., & Dufresne, A. (2009). Cellulose whiskers versus microfibrils: Influence of the nature of the nanoparticle and its surface functionalization on the thermal and mechanical properties of nanocomposites. *Biomacromolecules*, *10*(2), 425–432.

Siqueira, G., Bras, J., & Dufresne, A. (2010). New process of chemical grafting of cellulose nanoparticles with a long chain isocyanate. *Langmuir*, *26*(1), 402–411.

Siró, I., & Plackett, D. (2010). Microfibrillated cellulose and new nanocomposite materials: A review. *Cellulose*, *17*(3), 459–494.

Syverud, K., & Stenius, P. (2009). Strength and barrier properties of MFC films. *Cellulose*, *16*(1), 75–85.

Van Krevelen, D. W. (1997). *Properties of polymers* (3rd ed.). Amsterdam: Elsevier.